

A quantum enhanced search for dark matter axions

<https://doi.org/10.1038/s41586-021-03226-7>

Received: 24 July 2020

Accepted: 8 December 2020

Published online: 10 February 2021

 Check for updates

K. M. Backes^{1,6}✉, D. A. Palken^{2,3,6}, S. Al Kenany⁴, B. M. Brubaker^{2,3}, S. B. Cahn¹, A. Droster⁴, Gene C. Hilton⁵, Sumita Ghosh¹, H. Jackson⁴, S. K. Lamoreaux¹, A. F. Leder⁴, K. W. Lehnert^{2,3,5}, S. M. Lewis⁴, M. Malnou^{2,5}, R. H. Maruyama¹, N. M. Rapisarda⁴, M. Simanovskaia⁴, Sukhman Singh¹, D. H. Speller¹, I. Urdinaran⁴, Leila R. Vale⁵, E. C. van Assendelft¹, K. van Bibber⁴ & H. Wang¹

The manipulation of quantum states of light¹ holds the potential to enhance searches for fundamental physics. Only recently has the maturation of quantum squeezing technology coincided with the emergence of fundamental physics searches that are limited by quantum uncertainty^{2,3}. In particular, the quantum chromodynamics axion provides a possible solution to two of the greatest outstanding problems in fundamental physics: the strong-CP (charge–parity) problem of quantum chromodynamics⁴ and the unknown nature of dark matter^{5–7}. In dark matter axion searches, quantum uncertainty manifests as a fundamental noise source, limiting the measurement of the quadrature observables used for detection. Few dark matter searches have approached this limit^{3,8}, and until now none has exceeded it. Here we use vacuum squeezing to circumvent the quantum limit in a search for dark matter. By preparing a microwave-frequency electromagnetic field in a squeezed state and near-noiselessly reading out only the squeezed quadrature⁹, we double the search rate for axions over a mass range favoured by some recent theoretical projections^{10,11}. We find no evidence of dark matter within the axion rest energy windows of 16.96–17.12 and 17.14–17.28 microelectronvolts. Breaking through the quantum limit invites an era of fundamental physics searches in which noise reduction techniques yield unbounded benefit compared with the diminishing returns of approaching the quantum limit.

Almost a century after its existence was first postulated, dark matter, which makes up 27% of the Universe’s energy density, remains one of the most profound mysteries in fundamental physics¹². It determines cosmic structure formation and dominates the dynamics of galaxies, and there is overwhelming evidence that it cannot be composed of any particles described by the standard model of particle physics. Hypothetical particles called axions, originally proposed to solve the strong-CP problem in quantum chromodynamics (QCD)⁴, have emerged as leading dark matter candidates because experimental null results have placed stringent constraints on prominent alternatives¹³. If they exist, axions would probably be many orders of magnitude lighter than all massive standard model particles. In fact, they are sufficiently low-energy to behave like a weakly coupled oscillating field permeating all space. Investigating this field’s existence requires detectors sensitive to the axion’s coherent effects, rather than single-particle interactions. Recent years have seen a proliferation of detector platforms that are capable of probing different possible values of the axion mass^{14–17}. Among these, axion haloscopes^{3,8,18,19}, designed to search within the 1–50 $\mu\text{eV}/c^2$ mass range (c , speed of light in vacuum), are so far the only platforms to demonstrate sensitivity to the QCD axion.

An axion haloscope exploits the axion–photon coupling g , of the hypothetical axion field a to the pseudoscalar electromagnetic field product $\mathbf{E}\cdot\mathbf{B}$. It comprises a tunable, high-quality-factor (Q) cavity embedded in a large static magnetic field \mathbf{B} (ref. ²⁰), coupled to a low-noise readout system and held at a cryogenic temperature. An oscillating axion field generates a feeble oscillating electric field \mathbf{E} , which is resonantly enhanced when the frequency corresponding to the axion’s mass, $\nu_a = m_a c^2/h$ (h , Planck constant), falls within the bandwidth of a transverse magnetic TM_{0n0} -like mode²¹ of the cavity. The critical feature of axion searches is achieving sensitivity over a broad frequency range to detect a narrowband, axion-induced power excess of the order of 10^{-23} W at the unknown frequency ν_a .

The main figure of merit for a haloscope search is thus the scan rate R (in hertz per second) at which the detector can tune through frequency space for a given ratio of axion signal-to-noise power. Axion signal power in a haloscope is determined by the magnetic field, cavity performance and physical parameters of the axion field. With the signal power fixed by those quantities, a given haloscope has a quantum limited scan rate imposed by the zero-point fluctuations of the axion-sensitive cavity mode⁹. These fluctuations create a fundamental

¹Department of Physics, Yale University, New Haven, CT, USA. ²JILA, National Institute of Standards and Technology and the University of Colorado, Boulder, CO, USA. ³Department of Physics, University of Colorado, Boulder, CO, USA. ⁴Department of Nuclear Engineering, University of California, Berkeley, CA, USA. ⁵National Institute of Standards and Technology, Boulder, CO, USA.

⁶These authors contributed equally: K. M. Backes, D. A. Palken. ✉e-mail: kelly.backes@yale.edu

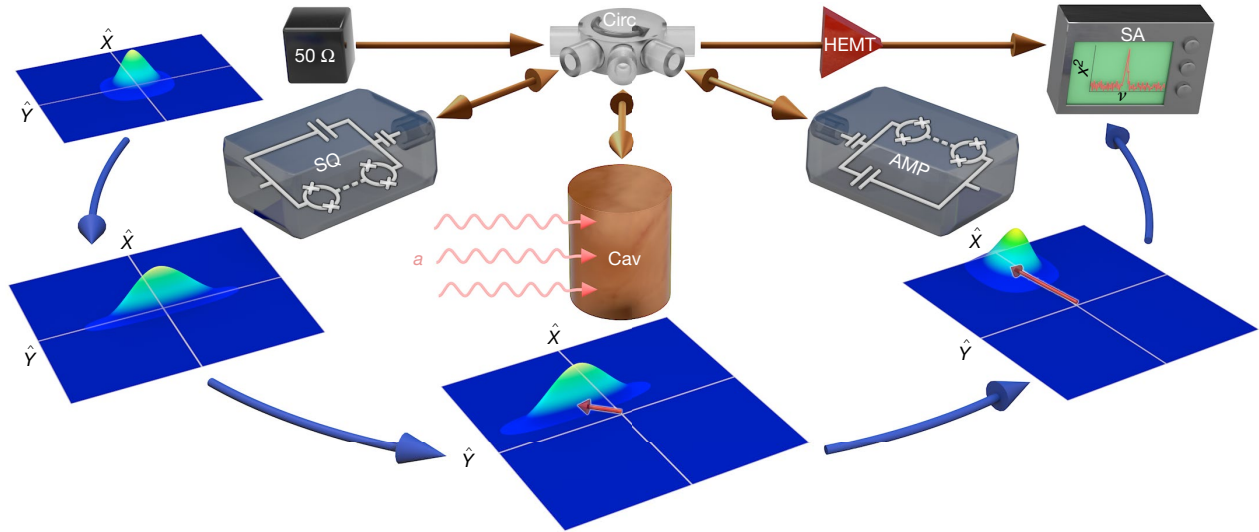


Fig. 1 | Illustration of the SSR-equipped haloscope, showing the transformation of the vacuum state in quadrature space. A vacuum state, the Wigner function (colour surface)³⁴ of which is symmetric in quadratures \hat{X} and \hat{Y} , is sourced as Johnson–Nyquist noise from a 50- Ω microwave termination (black box) at 61 mK. It is routed by a nonreciprocal element (Circ) to the SQ JPA, which squeezes the \hat{X} quadrature. The squeezed state may then be displaced by

a hypothetical axion field a in the axion cavity (Cav). It is subsequently unsqueezed by the AMP JPA, which in the process amplifies the axion-induced displacement along \hat{X} . The resulting state is measured by a conventional microwave receiver led by a high-electron-mobility transistor (HEMT) amplifier. The time record of many realizations of this process is Fourier-transformed for subsequent spectral analysis (SA).

barrier to improving haloscope scan rates that can only be overcome using quantum enhanced measurements²². Without a means of bypassing the quantum limit, the highly unfavourable $R \propto \nu^{-14/3}$ frequency scaling²³ of single-cavity haloscopes poses a stark challenge. At the quantum limit, scanning the 1–10 GHz frequency decade at the benchmark Kim–Shifman–Vainshtein–Zakharov (KSVZ)^{24,25} coupling g_{γ}^{KSVZ} would require hundreds of years of live time for today’s state-of-the-art haloscopes. Novel measurement technology is therefore needed to circumvent the quantum limit.

Here we report on a quantum enhanced axion search. The search was carried out with the Haloscope At Yale Sensitive To Axion Cold dark matter (HAYSTAC), which is designed to detect QCD axions in the range $m_a > 10 \mu\text{eV}/c^2$, which is favoured by recent calculations based on lattice classical field theory for the Peccei–Quinn field in post-inflationary Peccei–Quinn symmetry breaking scenarios, and assuming that axions saturate the cosmological dark matter density^{10,11} (alternative views should be noted, however; see for example ref. ²⁶). This work surpasses the quantum limit by coupling the HAYSTAC cavity to the squeezed-state receiver (SSR) shown in Fig. 1⁹. The SSR comprises two flux-pumped Josephson parametric amplifiers (JPAs)²⁷ coupled to the axion cavity via a microwave circulator. The first JPA, labelled the ‘squeezer’ (SQ), prepares a squeezed vacuum state, which is coupled into the axion cavity and subsequently measured noiselessly using the second, ‘amplifier’ (AMP), JPA. We achieve 4.0 dB of off-resonant vacuum squeezing, after the state is degraded by transmission losses and added noise, yielding a scan rate enhancement of a factor of 1.9 beyond what would have been achievable at the quantum limit. We observe no signature of dark matter axions in the combined 16.96–17.12 $\mu\text{eV}/c^2$ and 17.14–17.28 $\mu\text{eV}/c^2$ mass window for axion–photon couplings above $g_{\gamma} = 1.38 g_{\gamma}^{\text{KSVZ}}$, reporting exclusion at the 90% level.

The SSR¹ is coupled to the cavity, which is governed by the Hamiltonian

$$\hat{H} = \frac{h\nu_c}{2} (\hat{X}^2 + \hat{Y}^2), \quad (1)$$

where \hat{X} and \hat{Y} are the quadratures of the cavity field and obey $[\hat{X}, \hat{Y}] = i$, where i is the imaginary unit. The SQ, with half-pump frequency ν_p ,

centred on the cavity frequency ν_c , $\nu_p/2 = \nu_c$, performs a unitary squeezing operation on the electromagnetic field at its input, reducing the \hat{X} quadrature variance below vacuum and amplifying the \hat{Y} quadrature variance in accordance with the uncertainty principle. An axion field, if present, displaces the squeezed state along a random direction from the origin in the cavity field quadrature phase space via the inverse Primakoff effect²⁸. The displacement is proportional to the Lorentzian transmission profile of the cavity at ν_a and the square root of the axion-converted power²⁹. The squeezed quadrature is then amplified by the AMP via the inverse operation used to perform the squeezing. In the absence of any loss, the entire process is noiseless and unitary.

Squeezing improves the bandwidth over which the apparatus is sensitive to an axion, rather than its peak sensitivity, obtained at the cavity resonant frequency⁹. This bandwidth increase can be understood by considering the behaviour of the three distinct noise sources within a haloscope that obscure an axion-induced signal. The first is Johnson–Nyquist noise (which in the zero-temperature limit is vacuum noise), N_c , sourced from the internal loss of the cavity as a consequence of the quantum fluctuation-dissipation theorem. This noise is by definition inaccessible to the experimentalist and cannot be squeezed. It is filtered by the cavity response, giving it a Lorentzian profile at the cavity output. The second noise source is the system added noise, N_a , which encompasses the added noise of the entire amplification chain, including the AMP, referred to the input of the AMP. This noise source has historically been a dominant or co-dominant contribution^{8,18,19}, but here we operate our JPAs in a phase-sensitive mode, which can completely eliminate the contribution of this noise in one quadrature^{30,31} (switching from phase-insensitive to phase-sensitive operation on its own does not improve scan rate, but only phase-sensitive operation obtains a benefit from squeezing; see appendix C of ref. ⁹). In Methods, we show that our added noise is sufficiently small to be of negligible importance at all frequencies of interest. The third noise source is Johnson–Nyquist noise incident on and reflected off the cavity, N_r , which dominates away from cavity resonance. This noise is invariably present in any receiver configuration, and in our setup it is sourced from a 50- Ω termination held at the cryostat base temperature (61 mK). The ratio of the signal spectral density $S_{\text{ax}}(\delta_\nu)$ that would be delivered by an axion at any given detuning $\delta_\nu = \nu - \nu_c$ from cavity resonance to the cavity noise $N_c(\delta_\nu)$ is spectrally constant. Thus, the axion visibility $\alpha(\delta_\nu)$,

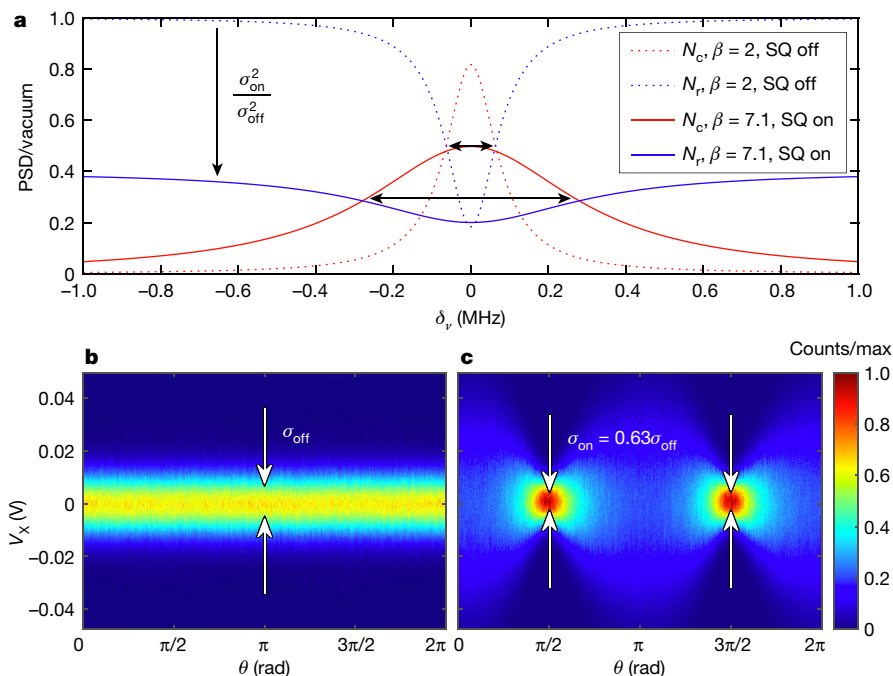


Fig. 2 | Advantage conferred by squeezing. **a**, Theory curves show the power spectral density (PSD) of Johnson–Nyquist noise reflected off the cavity (N_c ; blue) and generated within it (N_r ; red) at the cavity output, as a function of frequency. PSDs are normalized to the single-quadrature vacuum value of $\hbar\nu/4$. The solid and dashed lines are Lorentzian cavity response profiles obtained by optimizing the scan rate subject to squeezed and unsqueezed operation. Solid lines indicate the operating parameters used in this work and dashed lines indicate the coupling

configuration used in previous HAYSTAC operation³. The combination of squeezing and larger cavity coupling increases the bandwidth over which HAYSTAC is sensitive to axions. **b**, **c**, Voltage fluctuation (V_x) histograms as a function of the phase θ between the squeezer (SQ) and amplifier (AMP) pumps. In **b**, the SQ is turned off so that it reflects the vacuum noise untransformed, and the measured variance σ_{off}^2 is independent of the phase. In **c**, the SQ is turned on and the variance σ_{on}^2 is minimized to a value $< \sigma_{\text{off}}^2$ for $\theta = \pi/2$ and $\theta = 3\pi/2$.

defined as the signal-to-noise power spectral density ratio (neglecting transmission losses)

$$\alpha(\delta_v) = \frac{S_{\text{ax}}(\delta_v)}{N_c(\delta_v) + N_a(\delta_v) + N_r(\delta_v)}, \quad (2)$$

where all spectral densities, and hence α , are understood to refer to a single quadrature, is maximized on resonance, where N_c is the most dominant over N_r . Here, the denominator is the noise power spectral density, comprised of the sum of the three noise sources listed above. The maximum visibility $\alpha(0)$ occurs for an on-resonance axion signal. However, the scan rate R also depends on the bandwidth over which high visibility is maintained⁹,

$$R \propto \int_{-\infty}^{\infty} \alpha^2(\delta_v) d\delta_v. \quad (3)$$

By squeezing the reflected noise and taking α to be along the squeezed quadrature, the SSR does not improve the maximal visibility $\alpha(0)$, but rather increases the frequency range over which N_r is the dominant noise source, improving R and increasing the number of potential axion masses that are simultaneously probed at each cavity-tuning step.

Because squeezing reduces N_r in equation (2), it is beneficial to over-couple the cavity's measurement port relative to its internal loss rate in order to increase the measurement bandwidth⁹. The coupling ratio $\beta = \kappa_m/\kappa_l$, where κ_l is the internal dissipation rate and κ_m is the rate at which the cavity state decays out the measurement port, should be set to approximately twice the deliverable squeezing, defined as the SQ-on/off variance reduction at the system output, $S = \sigma_{\text{on}}^2/\sigma_{\text{off}}^2$. In Fig. 2a, the dashed lines show $N_c(\delta_v)$ in red and $N_r(\delta_v)$ in blue with $\beta = 2$ (ref. ³), the ideal coupling ratio for a quantum limited haloscope. The cavity noise N_c , emerging from the cavity in a δ_v -independent ratio with a hypothetical axion signal, is only dominant over the narrow band shown by the upper black arrow. The solid lines show the operating conditions

for this work, where squeezing is employed and the cavity is over-coupled at $\beta = 7.1$ (slightly higher than $2S$ owing to excess thermal noise; see Methods). Squeezing reduces the reflected noise, and increasing β to 7.1 increases the cavity bandwidth. Without squeezing, $\beta = 7.1$ would make cavity-reflected noise dominant at all frequencies. Squeezing this noise below the quantum limit yields high visibility that extends far off-resonance.

Figure 2b, c shows a direct measurement of the reduction in variance relative to vacuum in the amplified (\hat{X}) quadrature of the AMP, as a function of the phase θ between the SQ and AMP pumps. Noise is minimized when θ is an odd multiple of $\pi/2$, such that the AMP amplifies the quadrature that was initially squeezed. We automatically stabilize the phase by using a single microwave generator to source both pump tones. Comparing the amplified vacuum with the SQ on versus off, we measure a deliverable squeezing of $S = 0.40$ (equivalently, $-10\log_{10}S = 4.0$ dB) off the cavity resonance. Squeezing of N_r is benchmarked off-resonance, where it is the dominant noise. In practice, squeezing is limited by η , the transmissivity of the cables and microwave components between the SQ and AMP, scaling as $S = \eta G_s + (1 - \eta)$, where G_s is the inferred squeezing at the output of the squeezer, limited by saturation effects³¹. In the HAYSTAC system, $\eta \approx 0.63$, giving $S = 0.37$ as the theoretically optimal squeezing. This is nearly saturated by the measured value and corresponds to an almost twofold scan rate enhancement relative to optimal unsqueezed operation.

Using the SSR apparatus described above, we probed over 70 MHz of well motivated parameter space^{10,11} in half the time that would have been required for unsqueezed operation, saving approximately 100 days of scanning. Initial data acquisition occurred from 3 September to 17 December 2019, covering 4.100–4.178 GHz and skipping a transverse electric mode at 4.140–4.145 GHz that does not couple to the axion²¹. A total of 861 spectra were collected, of which 33 were rejected owing to cavity frequency drift, poor JPA performance or an anomalous power measurement in a probe tone injected near cavity resonance. Analysis

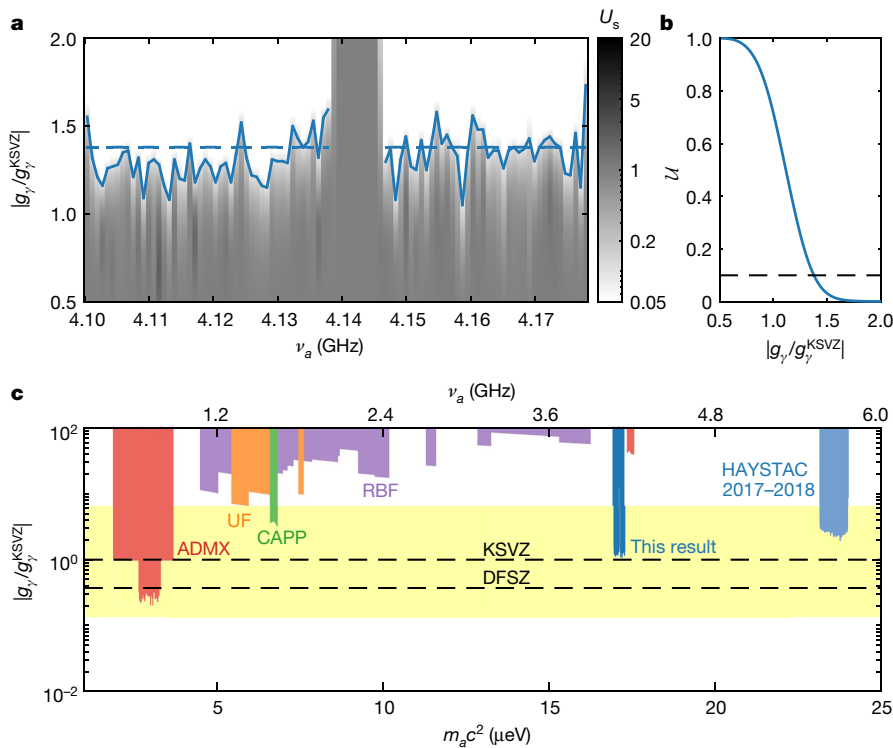


Fig. 3 | Axion exclusion from this work. **a**, Prior updates U_s in greyscale in the two-dimensional parameter space of axion frequency ν_a and coupling g_γ are achieved with a Bayesian analysis framework²³. The 10% prior update contour is shown in solid blue. The corresponding 90% aggregate exclusion level of $1.38 g_\gamma^{\text{KSVZ}}$ is shown by the dashed blue line. **b**, The frequency-resolved prior updates U_s are combined into a single aggregate prior update U as a function of coupling g_γ over the entire frequency range covered by the dashed blue line in

a, c, Results of this work are shown alongside previous exclusion results from the Axion Dark Matter eXperiment (ADMX), the University of Florida (UF), the Center for Axion and Precision Physics research (CAPP) and the Rochester–Brookhaven–Fermilab (RBF) collaboration (see ref.³⁵). The QCD axion model band representing the most natural KSVZ and Dine–Fischler–Srednicki–Zhitnitsky (DFSZ) models from a recent analysis³⁶ is shown in yellow, with the specific KSVZ^{24,25} and DFSZ^{37,38} model lines shown as black dashed lines.

of the initial scan data yielded 32 power excesses that merited further scanning, consistent with statistical expectations³². Rescan data were collected from 25 February to 11 April 2020. None of the power excesses from the initial scan persisted in the analysis of the rescan data. The process of optimizing the SSR as well as further measurements and calibrations taken periodically are described in Methods.

From these data, we report a constraint on axion masses m_a within the windows $16.96\text{--}17.12 \mu\text{eV}/c^2$ and $17.14\text{--}17.28 \mu\text{eV}/c^2$. Using the Bayesian power-measured analysis framework²³ described in Methods, we exclude axions with $g_\gamma \geq 1.38 g_\gamma^{\text{KSVZ}}$. Figure 3a shows in greyscale the prior update (change in probability) U_s that the axion resides at any specific location in parameter space, with the solid blue line showing the coupling for which $U_s = 10\%$ at each frequency. The aggregate update U (blue curve in Fig. 3b) to the relative probabilities of the axion and no-axion hypotheses corresponds to exclusion at the 90% confidence level over the entire window at the coupling for which $U = 10\%$. The results from our quantum enhanced data run are shown alongside other axion haloscope exclusion curves in Fig. 3c, including previous HAYSTAC results^{3,18} obtained using a single JPA near the quantum limit.

With these results, the HAYSTAC experiment has achieved a breakthrough in sensitivity by conducting a sub-quantum limited search for fundamental particles. Through the use of an SSR that delivers 4.0 dB of off-resonant noise variance reduction relative to vacuum, we have demonstrated record sensitivity to axion dark matter in the $10 \mu\text{eV}/c^2$ mass decade. This work demonstrates that the incompatibility between delicate quantum technology and the harsh and constrained environment of a real search for new particle physics can be overcome: in this instance, in an axion haloscope requiring efficient tunability and operation in an 8-T magnetic field. As intense interest in quantum information processing technology continues to drive

transmission losses downwards, quantum enhanced measurement will deliver transformative benefits to searches for new physics. In particular, the prospect of removing nonreciprocal signal routing, as could be accomplished by creating a parametric swap interaction³³ between the axion cavity and the JPA circuit, would boost transmission efficiencies above 90%, yielding a greater-than-tenfold scan rate increase beyond the quantum limit⁹.

Online content

Any methods, additional references, Nature Research reporting summaries, source data, extended data, supplementary information, acknowledgements, peer review information; details of author contributions and competing interests; and statements of data and code availability are available at <https://doi.org/10.1038/s41586-021-03226-7>.

- Slusher, R. E., Hollberg, L. W., Yurke, B., Mertz, J. C. & Valley, J. F. Observation of squeezed states generated by four-wave mixing in an optical cavity. *Phys. Rev. Lett.* **55**, 2409–2412 (1985).
- Tse, M. et al. Quantum-enhanced advanced LIGO detectors in the era of gravitational-wave astronomy. *Phys. Rev. Lett.* **123**, 231107 (2019).
- Brubaker, B. M. et al. First results from a microwave cavity axion search at $24 \mu\text{eV}$. *Phys. Rev. Lett.* **118**, 061302 (2017).
- Peccei, R. D. & Quinn, H. R. CP conservation in the presence of pseudoparticles. *Phys. Rev. Lett.* **38**, 1440–1443 (1977).
- Preskill, J., Wise, M. B. & Wilczek, F. Cosmology of the invisible axion. *Phys. Lett. B* **120**, 127–132 (1983).
- Dine, M. & Fischler, W. The not-so-harmless axion. *Phys. Lett. B* **120**, 137–141 (1983).
- Abbott, L. & Sikivie, P. A cosmological bound on the invisible axion. *Phys. Lett. B* **120**, 133–136 (1983).
- Braine, T. et al. Extended search for the invisible axion with the axion dark matter experiment. *Phys. Rev. Lett.* **124**, 101303 (2020).
- Malnou, M. et al. Squeezed vacuum used to accelerate the search for a weak classical signal. *Phys. Rev. X* **9**, 021023 (2019).

10. Buschmann, M., Foster, J. W. & Safdi, B. R. Early-universe simulations of the cosmological axion. *Phys. Rev. Lett.* **124**, 161103 (2020).
11. Klaer, V. B. & Moore, G. D. The dark-matter axion mass. *J. Cosmol. Astropart. Phys.* **2017**, 049 (2017).
12. Ade, P. A. et al. Planck 2015 results – XIII. Cosmological parameters. *Astron. Astrophys.* **594**, A13 (2016).
13. Bertone, G. & Tait, T. M. P. A new era in the search for dark matter. *Nature* **562**, 51–56 (2018).
14. Ouellet, J. L. et al. First results from ABRACADABRA-10 cm: a search for sub- μeV axion dark matter. *Phys. Rev. Lett.* **122**, 121802 (2019).
15. Majorovits, B. et al. Madmax: a new road to axion dark matter detection. *J. Phys. Conf. Ser.* **1342**, 012098 (2020).
16. Arvanitaki, A. & Geraci, A. A. Resonantly detecting axion-mediated forces with nuclear magnetic resonance. *Phys. Rev. Lett.* **113**, 161801 (2014).
17. Garcon, A. et al. The cosmic axion spin precession experiment (CASPER): a dark-matter search with nuclear magnetic resonance. *Quantum Sci. Technol.* **3**, 014008 (2018).
18. Zhong, L. et al. Results from phase 1 of the HAYSTAC microwave cavity axion experiment. *Phys. Rev. D* **97**, 092001 (2018).
19. Lee, S., Ahn, S., Choi, J., Ko, B. R. & Semertzidis, Y. K. Axion dark matter search around 6.7 μeV . *Phys. Rev. Lett.* **124**, 101802 (2020).
20. Sikivie, P. Experimental tests of the “invisible” axion. *Phys. Rev. Lett.* **51**, 1415–1417 (1983).
21. Rapidis, N. M., Lewis, S. M. & van Bibber, K. Characterization of the HAYSTAC axion dark matter search cavity using microwave measurement and simulation techniques. *Rev. Sci. Instrum.* **90**, 024706 (2019).
22. Caves, C. M., Thorne, K. S., Drever, R. W. P., Sandberg, V. D. & Zimmermann, M. On the measurement of a weak classical force coupled to a quantum-mechanical oscillator. I. Issues of principle. *Rev. Mod. Phys.* **52**, 341–392 (1980).
23. Palken, D. A. et al. Improved analysis framework for axion dark matter searches. *Phys. Rev. D* **101**, 123011 (2020).
24. Kim, J. E. Weak-interaction singlet and strong CP invariance. *Phys. Rev. Lett.* **43**, 103–107 (1979).
25. Shifman, M. A., Vainshtein, A. I. & Zakharov, V. I. Can confinement ensure natural CP invariance of strong interactions? *Nucl. Phys. B* **166**, 493–506 (1980).
26. Gorghetto, M., Hardy, E. & Villadoro, G. Axions from strings: the attractive solution. *J. High Energy Phys.* **2018**, 151 (2018).
27. Yamamoto, T. et al. Flux-driven Josephson parametric amplifier. *Appl. Phys. Lett.* **93**, 042510 (2008).
28. Primakoff, H. Photo-production of neutral mesons in nuclear electric fields and the mean life of the neutral meson. *Phys. Rev.* **81**, 899 (1951).
29. Al Kenany, S. et al. Design and operational experience of a microwave cavity axion detector for the 20 – 100 μeV range. *Nucl. Instrum. Methods Phys. Res. A* **854**, 11–24 (2017).
30. Caves, C. M. Quantum limits on noise in linear amplifiers. *Phys. Rev. D* **26**, 1817–1839 (1982).
31. Malnou, M., Palken, D. A., Vale, L. R., Hilton, G. C. & Lehnert, K. W. Optimal operation of a Josephson parametric amplifier for vacuum squeezing. *Phys. Rev. Appl.* **9**, 044023 (2018).
32. Brubaker, B. M., Zhong, L., Lamoreaux, S. K., Lehnert, K. W. & van Bibber, K. A. HAYSTAC axion search analysis procedure. *Phys. Rev. D* **96**, 123008 (2017).
33. Burkhart, L. D. et al. Error-detected state transfer and entanglement in a superconducting quantum network. Preprint at <https://arxiv.org/abs/2004.06168> (2020).
34. Braunstein, S. L. & van Loock, P. Quantum information with continuous variables. *Rev. Mod. Phys.* **77**, 513–577 (2005).
35. Tanabashi, M. et al. Review of particle physics. *Phys. Rev. D* **98**, 030001 (2018).
36. Di Luzio, L., Giannotti, M., Nardi, E. & Visinelli, L. The landscape of QCD axion models. *Phys. Rep.* **870**, 1–117 (2020).
37. Dine, M., Fischler, W. & Srednicki, M. A simple solution to the strong CP problem with a harmless axion. *Phys. Lett. B* **104**, 199–202 (1981).
38. Zhitnitsky, A. R. On possible suppression of the axion hadron interactions. *Sov. J. Nucl. Phys.* **31**, 260 (1980).

Publisher's note Springer Nature remains neutral with regard to jurisdictional claims in published maps and institutional affiliations.

© The Author(s), under exclusive licence to Springer Nature Limited 2021

Methods

Experimental operation

The HAYSTAC experiment, shown schematically in Extended Data Fig. 1, takes place in an LD250 BlueFors dilution refrigerator (with base temperature 61 mK) attached to an 8-T solenoidal magnet with a counter-wound bucking coil. The cavity sits at the centre of the high-magnetic field region, has volume $V_c = 1.5$ litres, unloaded quality factor $Q_0 = 2\pi\nu_c/\kappa_l = 47,000 \pm 5,000$ and TM₀₁₀ mode form factor $C_{010} \approx 0.5$. The cavity has two antenna ports²⁹. The first is a weakly coupled port used to input microwave tones to monitor gain stability and measure the cavity transmission profile. The second is a strongly coupled port that is used to read out from the cavity and for vector network analyser (VNA) scattering parameter measurements. The coupling of the coaxial antenna is mechanically actuated with a stepper motor. The two JPAs that comprise the SSR are held above the cavity inside a four-layer shielding can (niobium, Amumetal 4K; aluminium, Amumetal 4K; listed from inside to outside), surrounded by three superconducting bucking coils. This shielding is sufficient to reduce the flux through each of the superconducting quantum interference device (SQUID) loops of the JPAs to much less than one magnetic flux quantum, a roughly millionfold decrease in field strength from the high-field region 1 m below (the constraints of operation near an 8-T region were not present in the previous work described in ref.⁹). Inside the shielding can, each JPA has a current bias coil used to tune its resonance frequency. We tune the cavity by rotating an off-axis copper-plated tuning rod that occupies approximately one quarter of the cavity's volume using an Attocube ANR240 piezoelectric motor.

The experiment is operated in a series of discrete tuning steps. At each step, we actuate the piezo to tune the TM₀₁₀-like cavity mode, then extract the cavity resonance ν_c , the loaded quality factor $Q_l = 2\pi\nu_c/(\kappa_m + \kappa_l)$ and the coupling factor β using pairs of VNA measurements taken in transmission and reflection. To centre the amplification and analysis bands on the cavity resonance, we use a single microwave generator and a frequency divider to set the two JPA pump frequencies to $2\nu_c$ and the local oscillator used for homodyne measurement to ν_c . We set the gain of the AMP to $G_a \approx 28$ dB by adjusting the microwave generator amplitude and bias coil current. This corresponds to an AMP bandwidth of ~ 3 MHz. Both SQ (bandwidth ~ 26 MHz) and AMP therefore have bandwidths much greater than that of the cavity (bandwidth $(\kappa_m + \kappa_l)/2\pi \lesssim 1$ MHz). With the AMP gain set, the relative pump phase θ and amplitude are optimized to maximize squeezing using an electronically actuated variable phase shifter and attenuator. Simultaneously tuning the two JPAs and optimizing the squeezing at each frequency step poses new challenges that were not present in either the previous HAYSTAC runs^{3,18}, where only one JPA was used, or in the work of ref.⁹, where no tuning was performed. Axion-sensitive voltage fluctuations $V_x(t)$ are collected for $\tau = 3,600$ s in 720 5-s chunks. These chunks are further broken down into 10-ms segments before being Fourier-transformed, having their power spectral densities computed and being added to a running average. Each power spectrum then encompasses 3,600 s worth of data and is truncated to the analysis band of approximately 3 MHz centred on the cavity frequency.

To characterize our sensitivity to the axion, we perform calibrations once every nine tuning steps. The first step in our calibration protocol is a set of three power spectrum measurements to determine two experimental parameters: the noise spectral density,

$$N_{c0} = \frac{1}{2} \left(\frac{1}{2} + \frac{1}{e^{h\nu_c/k_B T} - 1} \right) = \frac{1}{4} \coth \left(\frac{h\nu_c}{2k_B T} \right), \quad (4)$$

generated within the cavity before being filtered by the cavity transmission profile (k_B , Boltzmann constant; T , temperature), and the squeezing $G_s(\nu)$ inferred at the output of the SQ. Measurement 1 is taken off the cavity resonance, with the squeezer turned off. Measurements 2 and 3 are taken on the cavity resonance with the squeezer turned on and off, respectively. From measurements 2 and 3 we infer a typical $G_s \approx 0.1$,

which corresponds to slightly less than the 4.0 dB of squeezing obtained in our off-resonant measurement of Fig. 2. From measurements 1 and 3 we calculate $N_{c0} = 0.41 \pm 0.02$ quanta, larger than the $N_f = 0.27$ quanta expected in thermal equilibrium with the cryostat base plate, owing to imperfect thermalization of the tuning rod. Because of this resonant excess over the noise sourced by the 50- Ω termination at the SQ input, which does equilibrate to the base temperature, the coupling of the strong port must be set to slightly higher than twice the deliverable squeezing S . Given this excess cavity noise, the optimal overcoupling for $S = 0.40$ is $\beta = 7.1$ instead of $\beta = 4.5$. Without squeezing, the optimal overcoupling in the presence of excess cavity noise is $\beta \approx 2.8$, slightly higher than the value of $\beta = 2$ plotted in Fig. 2. Fully accounted for, the cavity Johnson–Nyquist noise has negligible effect on the scan rate enhancement achieved via squeezing.

The second calibration measurement is a thermal calibration similar to the protocol used in previous HAYSTAC results^{3,31}, with a cold load at the dilution refrigerator base temperature and a hot load maintained at 333 mK (monitored by a Magnicon SQUID-based temperature sensor). This gives us the frequency-dependent, single-quadrature system added noise $N_a(\nu)$ referred to the input of the AMP. In our previous work, phase-insensitive JPA operation required the addition of $N_a \geq 1/4$ quanta per quadrature. Now, operating in phase-sensitive mode, we calculate the system noise referred to the AMP input to be $N_a = 0.03 \pm 0.02$ quanta averaged over the analysis band. These calibrations, together with system loss measurements taken *ex situ*, provide an accurate measurement of the total noise against which an axion signal must be measured.

Data analysis

Our data processing largely follows ref.³², and our analysis framework is that of ref.²³. The processing and analysis were separately performed by two semi-independent analysis teams at JILA and Yale, ultimately agreeing within 1% on the couplings excluded. The results presented in Fig. 3 are the average of the two analyses.

Coarse spectral structure and non-axionic power excesses are separately removed in both the intermediate frequency band (IF; zero frequency to megahertz) and the radio frequency band (RF; gigahertz). After cutting the spectra as discussed in the main text, we average the spectra in the IF band in order to extract shared non-axionic structure and power excesses. The shared structure in the IF band is a result of the shape of the receiver chain's spectral response and noise. An axion signal would line up in the RF band and wash out in the IF band, making it safer to remove power excesses in the IF band. We then remove remaining spectral structure wider than the axion (~ 9 kHz) from each individual spectrum, and perform cuts only on highly anomalous spikes that do not behave as axions in the RF band. Structure removal in both the IF and RF bands is done by dividing out Savitzky–Golay filters, equivalent to polynomial generalizations of moving averages in the frequency domain³². The remaining processed spectra consist of Gaussian-distributed noise with mean $\mu = 0$ (in the case that no axion is present) and standard deviation $\sigma = 1/\sqrt{\Delta_b \tau} = 0.0017$, where $\Delta_b = 100$ Hz is the Fourier bin size. Using maximum-likelihood weights determined from the noise calibrations described in the previous section and the parameters that determine axion signal power, we add these spectra together to produce a single combined spectrum. Again using maximum-likelihood weights, we then co-add groups of adjacent frequencies, taking into account the virialized axion lineshape³² in order to yield the final grand spectrum.

To test for the presence of an axion signature in the grand spectrum, we use the Bayesian power-measured analysis framework of ref.²³. The framework constitutes a straightforward application of Bayes' theorem that uses both the experimental sensitivity to the axion η_i (defined as the signal-to-noise ratio for an axion with coupling strength $g_i = 1$) and the actual excess power x_i measured at each frequency bin i to test for the presence or absence of the axion, taking advantage of the full information content of the measurement.

Article

The single-frequency, single-scan prior updates μ_i are defined as the change in probability of the axion existing at the i th grand spectrum bin due to the grand spectrum power x_i measured there. In the limit of low, but non-zero, prior probability of the axion residing anywhere in the scanned window, the prior probability itself drops out of the expression for the update. The update then reduces to the ratio of the no-axion (\mathcal{N}_i) to the axion (\mathcal{A}_i) probability distributions, which is well approximated as a Gaussian with $\sigma=1$ and $\mu_0=0$ (no-axion) or $\mu_a = g_{\nu,i}^2 \eta_i$ (axion), evaluated at x_i

$$u_i = \frac{P(x_i|\mathcal{A}_i)}{P(x_i|\mathcal{N}_i)} = \exp\left(-\frac{\mu_{a,i}^2}{2} + \mu_{a,i}x_i\right). \quad (5)$$

We multiply the updates from rescans onto the corresponding bins' initial scan updates to get the total updates U_i for each frequency bin. The resulting aggregate prior update,

$$u(g_\nu) = \frac{1}{N} \sum_{i=1}^N U_i(g_\nu), \quad (6)$$

which fully accounts for the look-elsewhere effect³⁹, falls below 10% at $g_\nu = 1.38g_\nu^{\text{KSVZ}}$ for the 4.100–4.140 GHz and 4.145–4.178 GHz combined frequency range shown in Fig. 3. In other words, the probability of an axion existing in our scan window at or above $1.38g_\nu^{\text{KSVZ}}$ has decreased by at least 90% as a result of our measurement. This corresponds to exclusion at the 90% confidence level in the sense reported in, for example, ref.¹⁸ (see appendix A of ref.²³). Finally, the subaggregated updates U_i shown in Fig. 3a apply the aggregation formula, equation (6), to 100 independent windows, each covering 1% of the width of the exclusion plot.

Data availability

The data central to the results of this manuscript are available from the corresponding author upon reasonable request.

Code availability

The custom codes used to produce the results presented in this manuscript are available from the corresponding author upon reasonable request.

39. Palken, D. A. *Enhancing the Scan Rate for Axion Dark Matter: Quantum Noise Evasion and Maximally Informative Analysis*. PhD thesis, Univ. of Colorado Boulder (2020).

Acknowledgements We acknowledge support from the National Science Foundation under grant numbers PHY-1701396, PHY-1607223, PHY-1734006, PHY-1914199 and PHY-2011357 and the Heising-Simons Foundation under grants 2016-044 and 2016-044. We thank K. Thatcher and C. Schwadron for work on the design and fabrication of the SSR mechanical components, F. Viemeyer for work on the room-temperature electronics and S. Burrows for graphical design work. We thank V. Bernardo and the J. W. Gibbs Professional Shop as well as C. Miller and D. Johnson for assistance with fabricating the system's mechanical components. We thank M. Buehler of Low-T Solutions for cryogenics advice. Finally, we thank the Wright laboratory for housing the experiment and providing computing and facilities support.

Author contributions K.M.B. ran the experiment with support from D.A.P., D.H.S., S.G., H.W., S.B.C., R.H.M. and S.K.L. Data were analysed by D.A.P. and K.M.B. with D.H.S., E.C.v.A. and H.W. contributing. K.M.B., M.M., D.A.P., S.M.L., N.M.R., A.D., D.H.S., E.C.v.A., R.H.M. and S.K.L. designed and assembled the experiment. D.A.P., M.M., B.M.B. and K.W.L. developed the squeezing concept. K.M.B. developed and implemented squeezing and other operational procedures with support from D.A.P., D.H.S., E.C.v.A. and H.W. The JPAs were designed by M.M., D.A.P. and K.W.L. and fabricated by L.R.V. and G.C.H. The cavity was designed and tested by N.M.R., S.M.L., S.A.K., H.J., A.F.L., M.S., A.D., I.U. and K.v.B. All authors, led by K.M.B. and D.A.P., contributed to the manuscript with figures created by S.G. and H.W.

Competing interests The authors declare no competing interests.

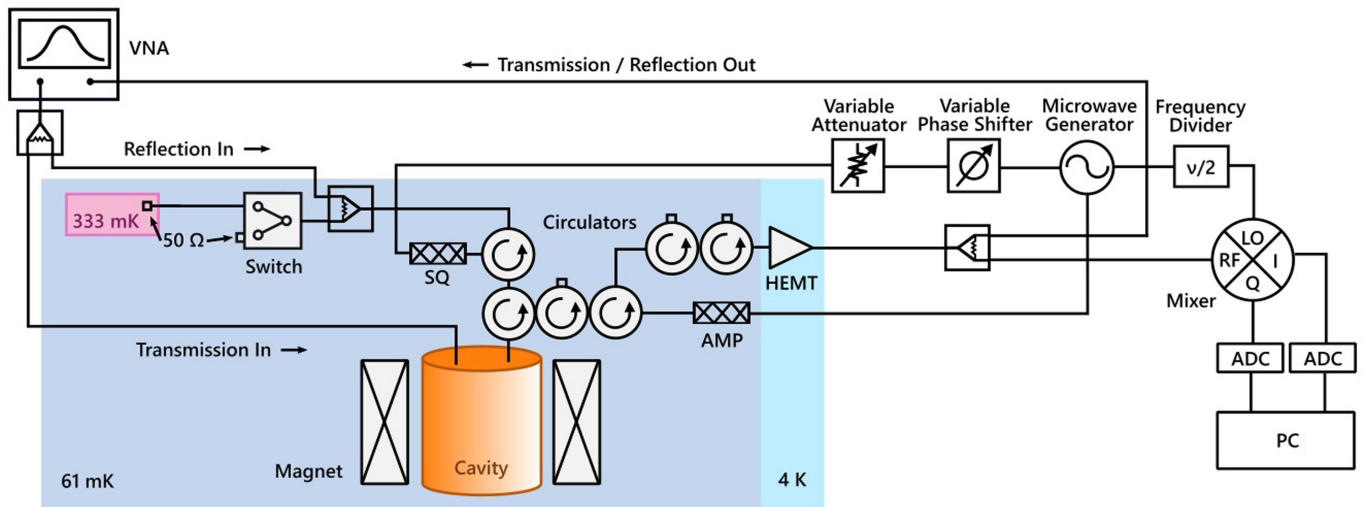
Additional information

Supplementary information The online version contains supplementary material available at <https://doi.org/10.1038/s41586-021-03226-7>.

Correspondence and requests for materials should be addressed to K.M.B.

Peer review information Nature thanks Igor Irastorza, David Marsh and the other, anonymous, reviewer(s) for their contribution to the peer review of this work. Peer reviewer reports are available.

Reprints and permissions information is available at <http://www.nature.com/reprints>.



Extended Data Fig. 1 | Simplified HAYSTAC experimental diagram. A single signal generator provides the local oscillator (LO) tone, as well as the tones for pumping both JPAs (SQ, AMP). Each JPA has two ports: one for the input of pump tones and one for input/output signals. The LO is set at half the pump frequencies via a frequency divider, and the relative phase and amplitude of the pump tones are set using a variable phase shifter and attenuator on the SQ pump line. Switches in the SQ and AMP pump lines (not shown) are used to toggle the JPAs on and off. Microwave circulators route signals nonreciprocally in order to realize the time sequence of operations illustrated in Fig. 1. Circulators with a 50-Ω termination on one port act as isolators, shielding

upstream circuit elements from unwanted noise coming from further down the measurement chain. During data acquisition and calibration measurements, signal and noise emitted from and reflected off the cavity are amplified by a HEMT amplifier at 4 K, fed into the RF port of an IQ mixer and mixed down to an intermediate frequency, digitized (ADC) and read into the computer (PC) where the power spectral density is calculated. The cavity's Lorentzian profile is monitored with reflection and transmission measurements taken using a VNA, for which a portion of the output is split off before the mixer. A switch that toggles between hot (333 mK) and cold (61 mK) 50-Ω loads is used for the calibration measurements described in the text.